Development of Activated Carbon Material from Oil Palm Empty Fruit Bunch for CO_2 Adsorption

Irsandi Dwi Oka Kurniawan[1], Randy Yusuf Kurniawan[1], Nurul Widiastuti[1], Lukman Atmaja[1], and Anis Shofiyani[2]
[1]Department of Chemistry, Institut Teknologi Sepuluh Nopember (ITS) 60111 Indonesia
[2]Department of Chemistry, Tanjungpura University, Pontianak
e-mail: irsandi.17012@mhs.its.ac.id; kurniawanrandy720@yahoo.com;
nurul_widiastuti@chem.its.ac.id; lukman_at@chem.its.id; anis.shofiyani@chemistry.untan.ac.id

***Abstract*— This study aims to determine the CO2 adsorption capacity of activated carbon doped with nitrogen. Activated carbon is carbonized from oil palm empty fruit bunches (OPEFB). The results of lignocellulose analysis from OPEFB, 42.87 wt% of hemicellulose, 27.31 wt% of lignin, 23.03 wt% of cellulose and 2.77 wt% of ash. Potassium hydroxide is used as an activating agent and urea as a nitrogen precursor with an OPEFB mass: urea is 1: 1 to 1: 5. The method used is single-step, where carbonization-activation-doping is made into one process. Activated activated carbon is characterized by Fourier-Transform Infrared (FTIR), X-ray diffraction (XRD), Brunauer–Emmett–Teller (BET) isotherm, and scanning electron microscope (SEM) with energy dispersive X-ray. Infrared spectra showed that N-doped activated carbon was successfully synthesized. Diffractogram shows an amorphous structure with graphitic plane (002) and (100). ACN11 produces the highest surface area of 1309.47 m2 g-1. The results of gravimetric CO2 adsorption at 30 °C and 1 atm conditions resulted in the largest CO2 adsorption capacity of ACN14 at 15.02 wt%. The ACN11 and ACN14 adsorption kinetics models followed the intraparticle diffusion model with R2 values of 0.95 and 0.97.**

***Keywords*—Empty Fruit Bunch, N-Doped Activated Carbon, Urea, Single-Step Method, Gravimetric, CO2 Adsorption.**

I. INTRODUCTION

Global warming occurs because of the trapping of sunlight on the earth's surface, so that the temperature of the Earth's atmosphere increases. The capture of sunlight radiation is caused by the effects of greenhouse gases[1]. Gases are included in greenhouse gases such as carbon dioxide (CO_2), methane (CH_4), nitrogen oxide (NO_x) and fluorine. Increased impact of global warming due to increased CO_2 gas emissions because 81% of greenhouse gases are CO_2.The increasing concentration of CO_2 emissions in the atmosphere occurs due to emissions from the production and use of incandescent bulbs of 1.6 tons CO_2/year, motorized vehicles of 3.0 tons CO_2/year and industrial waste (including households) of 4.5 tons CO_2/year . Research reports that in 2010 the average atmospheric CO_2 content was 380 ppm with an average temperature increase of 14.5 °C and it is estimated that at 2045 the CO_2 content in the atmosphere will reach 450 ppm with an average temperature increase of around 14.6 °C [2].

CO_2 emissions in the atmosphere can be reduced by increasing energy conversion efficiency, using other energy sources such as solar energy, nuclear energy, and CO_2-based biomass-based fuels. Wang, et al. (2011), reported that this fuel source cannot replace fossil fuels at this time on a large scale because of the high costs of the production process[3]. Several methods have been reported to reduce CO_2 gas emissions, such as solvent absorption, separation using membranes, adsorption using solid sorbents and cryogenic separation. Solvent absorption with amine based is widely used in chemical plants to process large amounts of emissions from power plants because of the high efficiency of the process[4], [5]. Although efficiency is high, intensive energy consumption is also high for solvent regeneration, corrosion of equipment, processing and high volatility[6], [7]. The most relevant method used is adsorption using solid sorbent which has more advantages such as easy handling, high adsorption capacity and selectivity, long-term stability, low energy regeneration, and low costs[8].

Some porous material that has been reported for CO_2 adsorption, such as Organic Material Frameworks (MOFs), Zeolitic Imidazolate Frameworks (ZIFs), Porous Organic Polymers (POPs), Covalent Organic Frameworks (COFs), mesoporous silica, chitosan zeolite composites and activated carbon[9]. MOFs, POPs, and COFs have complex synthesis, high prices, low adsorption capacity under low pressure[10], mesoporous silica has poor selectivity[11], ZIFs have low adsorption capacity at low pressure and low thermal stability[12], zeolites are not water resistant and unstable under acidic or alkaline conditions[13], porous carbon has a low adsorption capacity. However, carbon has the potential to be used as an adsorbent under conditions of low pressure and room temperature [14] and has an easily modified pore structure and size. Selective carbon with CO_2 and can be easily regenerated, unlike other physical adsorbents such as zeolites or MOFs, both hydrophobic and high stability in humid conditions[15]. Carbon also has a high surface area which is between 300-1000 $m^2\ g^{-1}$, economical and has good recycling properties[16], [17]. Carbon can be obtained from biomass containing lignocellulose and then hydrolyzed at high temperatures (600-900 °C) in the flow of N_2 gas to damage its structure into structures with the dominant structure of carbon-carbon bonds[18].

Carbon from oil palm biomass can be produced through high temperatures to degrade lignocellulose structures from their raw materials to carbon material. Evbuomwan, et al. (2013) reported that the activation of single-step activated carbon from oil palm using $NaHCO_3$ resulted in a BET surface area of 1080 $m^2\ g^{-1}$ [19]. Hussaro, (2014) reported that BET surface area for activated carbon which when activated using Na_2CO_3 was 742.43 $m^2\ g^{-1}$ and $ZnCl_2$ amounted to

551.05 m^2 g^{-1} [20], while activation with KOH produced a BET surface area of 1250 m^2 g^{-1} [21], 1408 m^2 g^{-1} [22], 1621 m^2 g^{-1} [23] and 1704 m^2 g^{-1} [24]. Based on the description above, the activating agent in the form of KOH produces a BET surface area of more than 1000 m^2 g^{-1}.

Research on carbon-based adsorbents tried to increase chemisorption through nitrogen doping because CO_2 has acidic properties and nitrogen atoms induce basicity in order to create CO_2-philic sites by increasing surface polarity, electrical conductivity, and the tendency of electron-donors from porous carbon[25]. Usually, three basic criteria are involved for CO_2 adsorption including high adsorption capacity, stable recyclability and high selectivity. Increasing selectivity through structural modification is considered an effective solution by doping heteroatoms such as nitrogen into the carbon matrix. The results of Liu's study, et al., (2015), reported that activated carbon doped with nitrogen from urea with a ratio of carbon:urea = 1:1 and 1:2, respectively had an adsorption capacity of 4.6 and 3.7 mmol g^{-1} with selectivity of 45[26], compared to activated carbon without nitrogen doping only has a selectivity of 5.4 with an adsorption capacity of 4.8 mmol g^{-1} [3]. From these data it can be seen that nitrogen doping on activated carbon does not significantly reduce the adsorption capacity and increase the selectivity value of CO_2 adsorption. In this study, variations in the mass of carbon: urea, ie 1: 1, 1: 2, 1: 3, 1: 4 and 1: 5 were used to determine the effect of adding nitrogen doping to CO_2 adsorption capacity. Adsorption kinetics model was also investigated to determine the adsorption rate of the material synthesized.

II. METHOD

A. Materials

The materials used in this study were oil palm empty fruit bunches biomass from Pontinak, Kalimantan Barat, Indonesia, acetone (pa, CAS no. 666-52-4), sodium hydroxide (NaOH 99% pa, Merck), potassium hydroxide (KOH 99% pa, Merck, 1310-58-3), demineralized water, H_2SO_4 (98% pa), N_2 Ultra High Purity (UHP) gas (99.9999% N2), Chloride acid (HCl 37%, SAP), urea (CAS no. 57-13-6, Merck) and CO_2 Ultra High Purity (UHP) gas (99.9999%).

B. Analysis of Lignocellulose

Lignocellulose content analysis using the Chesson-Datta method from Isroi et al., (2012). OPEFB are cut into small pieces and then washed with demineralized water and dried under the sun for 8 hours/day for 3 days. Next, the sample is heated in an oven at 105 °C for 24 hours. 1 gram of OPEFB wrapped into the acetate thimble and placed in the reflux component. 150 mL of water was added to the round bottom flask then heated at 100 °C for 2 hours. Then the sample is filtered and dried in an oven at 105 °C for 2 hours. Reflux continuously until the percentage of lignin, hemicellulose, cellulose and ash is obtained[27].

C. Single-step Pyrolysis

Single-step pyrolysis includes the stages of carbonization, nitrogen doping, and chemical activation which are made into one process[21], [28]. The ratio of carbon precursors and chemical activating agents KOH is 1: 3 with variations in the ratio of carbon precursors to urea masses of 1: 1, 1: 2, 1: 3, 1: 4, 1: 5. Then the sample was hydrolyzed at 800 °C with a holding time of 3 h and the heating rate was 10 °C min^{-1}. Carbon material was obtained, then washed several times using 10 wt% of HCl and washed with demineralized water to neutral pH. The modified carbon obtained is denoted as ACN-x-y. Variable x is the mass ratio of OPEFB and y is the mass ratio of urea are used.

D. Characterization of Materials

Identification of functional groups on carbon materials using the Nicolet iS 10 FT-IR Spectrometer. The spectra were recorded in the range of 4000-500 cm^{-1}. Pellet discs were prepared by mixing dried biomass samples with KBr spectroscopic grade salt in granite mortar. The pellet was then pressed at 1 MPa for about 10 min before reading the spectra. X-ray diffractometer (XRD) with Copper anode (Cu-Kα, λ = 1.5406) was used to identify the formed phases in the ACN sample.

The morphology of N-doped activated carbon can be detected through SEM-EDS method. The sample is placed on the surface of the holder who has been given a carbon tape, then gold is coated on the surface of the sample. After coating, the sample is inserted in the sample room which has been vacuumed first, then the sample is analyzed using a SEM instrument (HITACHI FLEXSEM 100) to find out the morphology.

Porosity is measured using surface area and porosity analyzer (Quantachrome Instruments, ASAP2020). The gas used for analysis is N_2 at -195 °C. Before the measurement process is carried out, each sample is degraded at 300 ° C overnight. Surface area (S_{BET}) is calculated using the BET (Brunauer-Emmett-Teller) method in the range of relative pressures of 0.05 to 0.25. The total pore volume (V_{tot}) is obtained at P/P_0 = 0.995. The t-plot method is used to calculate the micropore volume (V_{micro}). Pore size distribution (PSD) is obtained from N_2 gas desorption data and using SAIEUS Software with 2D-NLDFT[29].

E. CO_2 Adsorption Measurement

Measurement of CO_2 adsorption capacity using the gravimetric method by weighing 0.5 g of the sample then degraded at 300 °C for 3 hours. The measurement process is carried out at 30 °C under a pressure of 1 atm. The CO_2 flow rate during the adsorption process is controlled at 20 mL min^{-1}. Changes in mass are recorded by the analytical balance of Ohaus Pioneer. The scheme of the tools used in this study is illustrated in Figure 1.

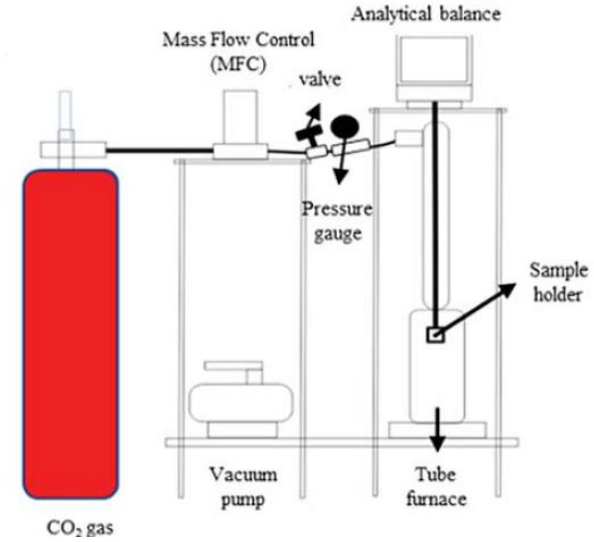

Figure 1. Schematic diagram of the adsorption system

Eqn (1) was used to determine the weight of adsorbed CO_2:

$$CO_2\ wt\% = \frac{M_{eq}-M_0}{M_0+(M_{eq}-M_0)} \times 100\% \quad (1)$$

where M_{eq} is the mass after adsorption reached equilibrium and M_0 is the initial mass of the adsorbent after degassing process[30].

F. Adsorption Kinetics

Kinetic models are used to determined gas transport mechanisms and adsorption types of CO_2 into adsorbent based-carbon. In this study, pseudo-first order and pseudo-second-order models were used[31], [32].

Pseudo-first order is the model used to describe the adsorption process is given by eqn (2):

$$\ln(q_e - q_t) = \ln q_e - k_f t \quad (2)$$

where q_t (mmol g^{-1}) is the amount of adsorbate adsorbed at the time of t (minute), q_e (mmol g^{-1}) is the adsorption capacity at equilibrium and k_f (min^{-1}) is the rate constant of the pseudo-first order.

Pseudo-second order can be determined using eqn (3):

$$\frac{dq_t}{dt} = k_s(q_e - q_t)^2 \quad (3)$$

After integrating and applying boundary conditions, the equation can be integrated further with the initial condition of $q_t = 0$ at $t = 0$ and $q_t = q_t$ at $t = t$. A linear equation can be obtained

$$\frac{t}{q_t} = \frac{1}{k_s q_e^2} + \frac{1}{q_e} t \quad (4)$$

and the initial sorption rate, h (mg g^{-1} min^{-1}) as $t \rightarrow 0$ can be defined as

$$h = k_s q_e^2 \quad (5)$$

Intraparticle diffusion was used to determine the adsorption process in porous materials and is expressed in eqn (6):

$$q_t = k_{id} t^{1/2} + C \quad (6)$$

Where, t is time (min). The diffusion constant k_{id} (mmol g^{-1} $min^{-0.5}$) can be determined experimentally from the slope of the plot of q_t versus $t^{1/2}$, and C is an intercept that expresses the thickness of boundary layer[33].

III. Results and Discussion

A. Lignocellulose Content

Table 1 presents data on the content of lignocellulose (lignin, cellulose, hemicellulose) and ash in OPEFB.

Table 1.
Lignocellulose Content of OPEFB

	Content (wt%)
Lignin	27.31
Hemicellulose	42.87
Cellulose	23.03
Ash	2.77
Yield	61.49

Analysis of lignocellulose content using the Chesson-Datta method obtained hemicellulose by 42.87 wt%, lignin at 27.31 wt%, cellulose at 23.03 wt%, and ash at 2.77 wt% for OPEFB from Pontianak, West Kalimantan, Indonesia. Sutikno, et al., (2017) reported that the lignocellulose content of OPEFB fibers from Central Lampung was 28.60 wt% hemicellulose, 42.30 wt% cellulose and 22.40 wt% lignin[34]. The lignocellulose content of each OPEFB differs from the origin of the OPEFB region. The amount of lignin content in cellulose determines the amount of carbon produced during the pyrolysis process. While the content of hemicellulose and cellulose determines the surface area produced, the higher the content of hemicellulose and cellulose, the higher the surface area[35]. Cellulose and lignin have a high resistance to KOH, this is related to the mass of carbon produced from OPEFB at 61.49 wt%.

B. Identification of Functional Groups and Adsorbent Structures

Figure 2 shows FTIR spectra of each sample. OPEFB samples showed an absorption band at 3227.05 cm^{-1} indicating a vibrational functional group of the hydroxyl OH strain with a wide and clear peak[36], 2918.06 cm^{-1} indicating CH strain vibration with medium intensity, 1628.97 cm^{-1} indicates strain vibration C = C stretching with medium intensity and 1030.52 cm^{-1} indicates CO strain stress with strong intensity[37]. Whereas, carbon which is the result of pyrolysis (without activation and doping) at a temperature of 800 °C peak O-H, C-H and C-O disappears but the peak C=C is still visible even though the intensity decreases.

There are no peaks produced by ACN13 and ACN15, as seen in OPEFB and carbon. Based on Figure 2, the addition of the mass ratio of urea as a nitrogen doping precursor has a similar trend. During the process of carbonization, activation, and doping most of the functional group absorption peaks disappear. This is because the functional groups of the spectrum of raw materials are evaporated as volatile materials when high heat (up to 800 °C) is supplied to the sample[38]. This proves that the activation process has been successfully carried out.

Figure 3 shows a diffractogram pattern for ACN13 and ACN15. There is no sharp characteristic peak observed in the diffractogram. However, two wide peaks were found at 27.3° and 44°. These two angles are respectively graphical fields (002) and (100). A similar XRD pattern was observed for activated carbon originating from palm fiber using the single-step pyrolysis method[28]. This shows that ACN produced from a single-step activation process is somewhat amorphous but may have several microcrystalline structures. This XRD pattern shows that the activated carbon shows an irregular turbostatic structure of carbon material[39]. The turbostatic structure is a layer of microcrystalline interference formed because of the presence of heteroatoms such as hydrogen, oxygen, nitrogen or empty lattice cavities in activated carbon. The peak and diffractogram intensity formed at ACN15 are lower than ACN13, this is due to KOH activation and nitrogen doping leading to uniform destruction of the structural domain and random distribution of carbon atoms. Amorphous activated carbon pores function as active sites for the adsorption of ions or molecules, while layers that have crystal structures tend to be more appropriately used for electron transfer channels during electrochemical processes[40].

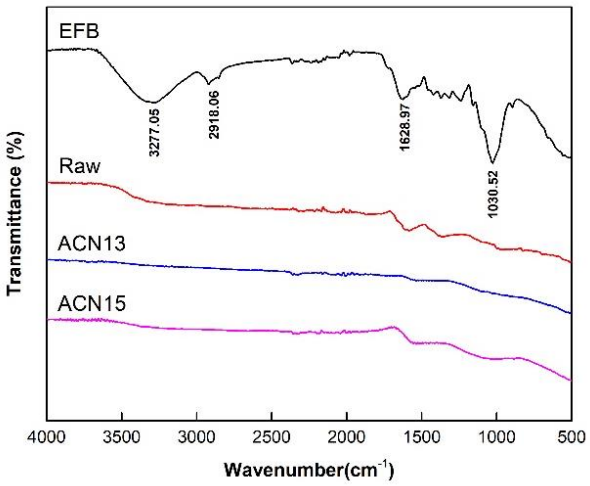

Figure 2. FTIR spectra of OPEFB, raw, ACN13 and ACN15

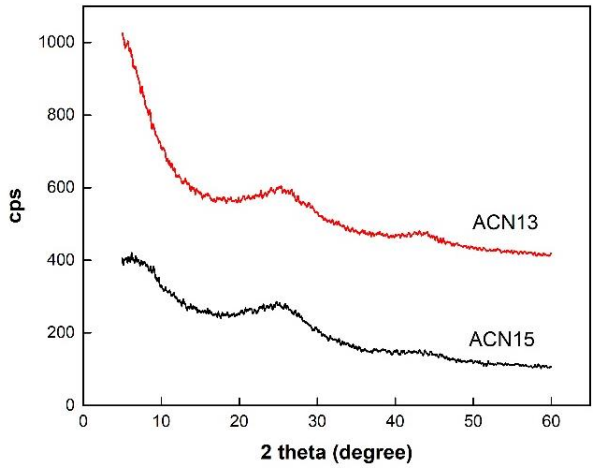

Figure 3. Diffractogram XRD of ACN13 and ACN15

C. *Surface Morphology*

Figure 4 shows the morphology of the carbon material produced during pyrolysis of 800 °C. Carbon morphology which is hydrolyzed at 800 °C without treatment KOH activation and nitrogen doping is shown in Figures 4.a and 4.b. In figure 4.b with a magnification of 1000x, it can be seen that the carbon pores formed on the surface are very irregular or not too many pores are formed. Whereas, in Figures 4.3 (c) and 4.d, it shows the morphology for ACN14 samples given KOH activation treatment and nitrogen doping with carbon mass ratio compared to urea = 1: 4 formed pores in the front cross section.

The results of SEM EDS using Cu-Kα rays for ACN14 samples are shown in Figure 4.e carbon elements, 4.f nitrogen elements, 4.g oxygen elements. The content of each detected element is shown in Figure 4. h with values of 70.45 wt% carbon, 18.41 wt% oxygen, 7.85 wt% nitrogen, and 3.29 wt% potassium. The results of EDS showed that the carbon pore material was successfully activated using KOH with nitrogen doping of 7.85 wt% and a small amount of K of 3.29 wt%.

The mechanism of the promotion and inhibition effect on nitrogen doping is the same as the effect on surface area. For the two-step method, then doping activation can destroy many functional groups containing oxygen, leaving carbon "non-active" in the inert atmosphere, so that the amount of nitrogen in the sample can be lower than before. formed during activation using KOH can also inhibit the formation of carbon so that the number of pores produced becomes less. Some samples that become "non-active" carbon because the formation of K_2CO_3 also has a portion of nitrogen mass, so that the insertion of heteroataom nitrogen becomes ineffective. nitrogen contained in the K_2CO_3 sample is higher than that produced by KOH activation[41].

D. *N_2 Adsorption-Desorption Isotherm*

Figure 5 shows that the isotherms that occur during the adsorption-desorption process of nitrogen from carbon materials with OPEFB precursors are included in type I isotherms based on the classification of the International Union of Pure and Applied Chemistry (IUPAC). Usually, type I isotherms display convex curves and this type of platform exits horizontally or almost horizontally, and the adsorption isotherm directly intersects with line $P/P_0 = 1$ [38]. The highest nitrogen adsorption-desorption volume is owned by ACN14 and ACN15 by following type I isotherms, adsorption which occurs in pore averages which are included in micropore (diameter < 20 Å). Although the isotherm curves for ACN11 to ACN15 samples with higher urea mass ratios show very small hysteresis loops, which are indicative of type IV, they still resemble type I [21].

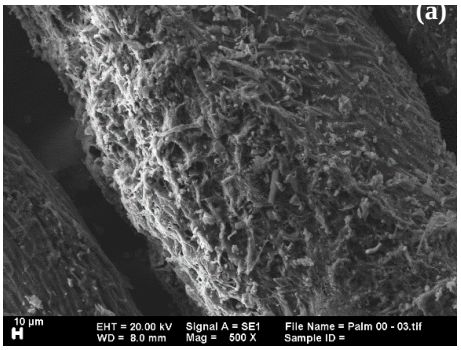

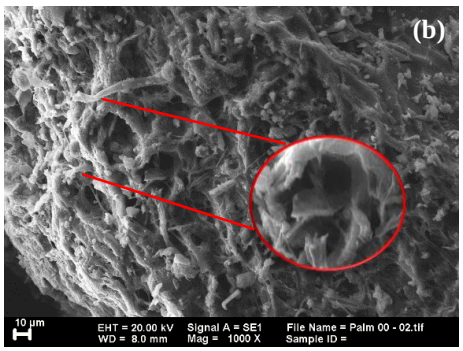

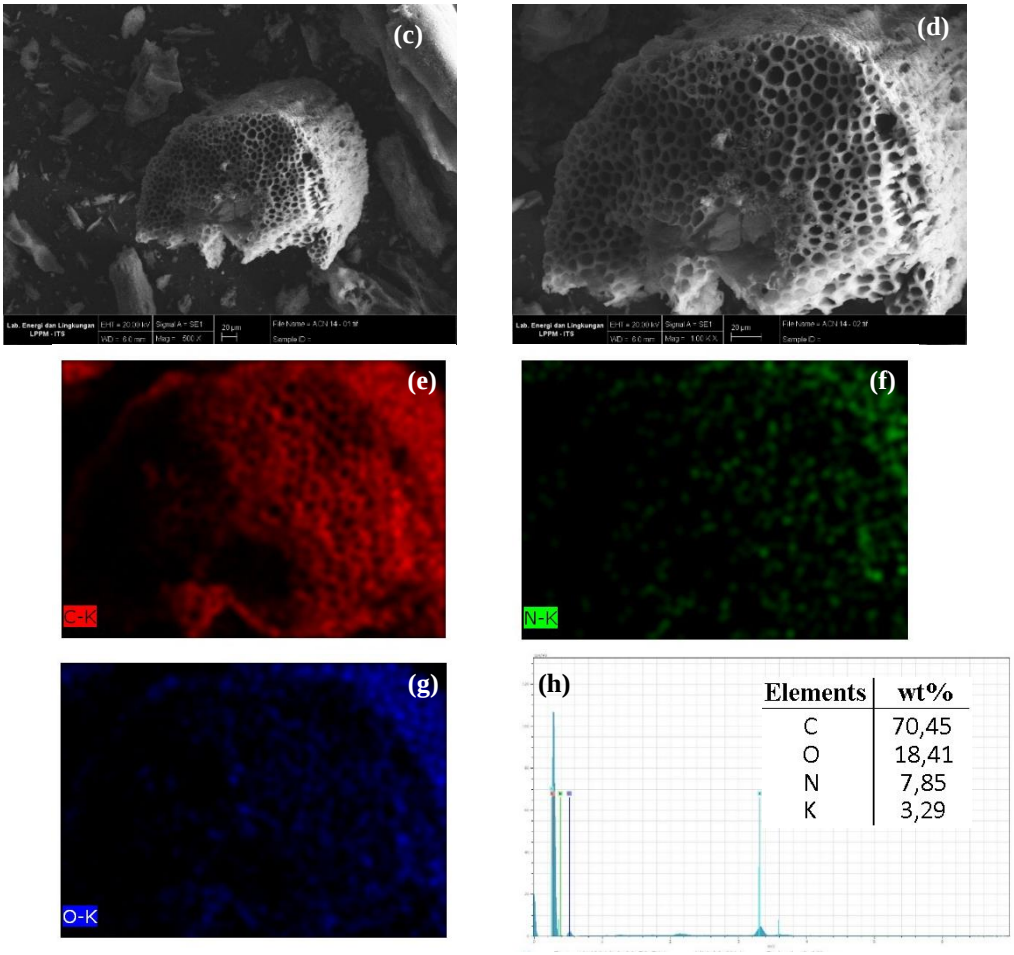

Figure 4. Morphology of SEM (a) Carbon (without activation and doping) 500x magnification, (b) Carbon (without activation and doping) 1000x magnification, (c) ACN14 500x magnification, (d) ACN14 1000x magnification, EDX from ACN14 (e) carbon element , (f) element of nitrogen, (g) element of oxygen, and (h) percentage of content of each element obtained.

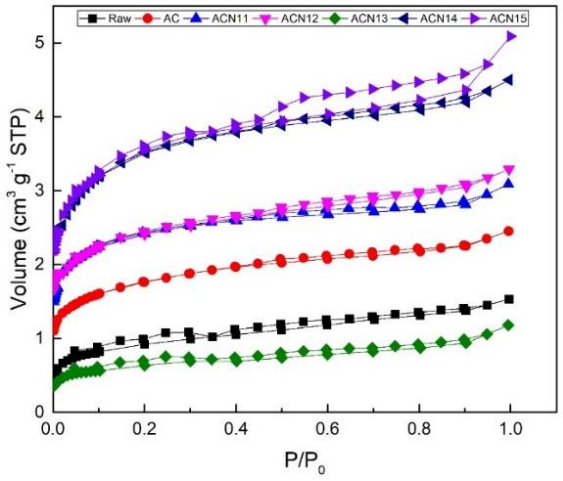

Figure 5. Adsorption-desorption N_2 isotherm

The surface properties of carbon, activated carbon, ACN11 to ACN15 are summarized in Table 2. The highest surface area calculated using the BET (S_{BET}) method is found in ACN11 of 1309.47 m^2 g^{-1} and ACN14 of 1230.30 m^2 g^{-1}. Comparable to the value of the surface area produced, the total pore volume (V_{tot}) of ACN11 and ACN14 were 0.114 cm^3 g^{-1} and 0.096 cm^3 g^{-1}, respectively. Comparison of the surface area produced between carbon, activated carbon (AC) and ACN11 has a significant difference. This shows that with activation followed by doping can increase the surface area (S_{BET}; 217.54 < 699.14 < 1309.47 m^2 g^{-1}) and increase the micropore volume (V_{micro}; 0.17 < 0.52 < 0, 84 cm^3 g^{-1}) on the surface of the carbon material produced. When the temperature increases, the amount of nitrogen inserted into carbon particles also increases. This is due to (i) formation of micro cracks due to higher internal pressure on carbon at higher temperatures and (ii) degradation of cellulose content from biomass particles at higher temperatures from 210-220 °C [41]. Continuous increases in temperature causing urea decomposition reactions take place through pyrolysis which may occur at temperatures between 350 °C and 400 °C [42]. The gases released during pyrolysis are proposed as a key step to open parallel channels and develop pores of different sizes, followed by the activation process simultaneously by raising the temperature to 800 °C.

Table 2.
Properties of the Surface of Carbon Material from OPEFB Precursors which are Pyrolyzed by a Single-Step Method at 800 °C

Sample	S_{BET} (m^2 g^{-1})	V_{tot} (cm^3 g^{-1})	V_{micro} (cm^3 g^{-1})	V_{meso} (cm^3 g^{-1})	Average Pore Radius (Å)
Raw	217.54	0.17	0.15	0.02	15.79
AC	699.14	0.52	0.45	0.07	14.90
ACN11	1309.47	0.84	0.72	0.11	12.80
ACN12	1009.85	0.69	0.60	0.08	13.62
ACN13	332.10	0.29	0.24	0.05	17.46
ACN14	1230.30	0.78	0.69	0.10	12.71
ACN15	875.03	0.62	0.52	0.10	14.06

However, the amount of nitrogen inserted can be reduced if the domain of K_2CO_3 formation is higher. In this study using a carbon mass ratio compared to KOH of 1:3 and mass doping of nitrogen from urea varied from 1 to 5. In ACN11 the BET surface area is higher than the other samples, followed by total volume, micropore and mesoporous highest too. ACN14 ranks second with the highest score. Whereas, for ACN13 it has the lowest value with a surface area of 332.10 $m^2 g^{-1}$, total volume of 0.29 $cm^3 g^{-1}$, micropore volume of 0.24 $cm^3 g^{-1}$, and mesoporous volume of 0.05 $cm^3 g^{-1}$. This value is smaller than activated carbon (with KOH activation) without nitrogen doping treatment. In terms of mass ratio between KOH as an activating substance and urea as a nitrogen precursor it can cause fewer carbon pores to be formed, because the complex thermal decomposition of urea produces products such as ammonia and carbon dioxide[43], thereby increasing the formation of K_2CO_3. Excess carbon dioxide encourages the formation of K_2CO_3 in the one-step pyrolysis process, so that the character of the carbon formed becomes less good[15].

The pore distribution shown in Figure 6 is pore distribution desorption data using the BJH method (Barrett, Joyner, and Halenda) for each sample of carbon material from the OPEFB. Carbon samples and activated carbon each have a mean pore radius of 15.79 and 14.90 Å and a micropore volume of 0.15 and 0.45 $cm^3 g^{-1}$, respectively. While for ACN11 and ACN14, each pore radius has an average of 12.80 and 12.71 Å and the micropore volume is 0.72 and 0.69 $cm^3 g^{-1}$, respectively. This is also because the surface area of ACN11 and ACN14 is greater than carbon and activated carbon, so the micropores owned by ACN11 and ACN14 are greater than carbon and activated carbon. Whereas for ACN13 samples which have a micropore volume of 0.24 $cm^3 g^{-1}$ are between carbon and activated carbon, so the number of micropores based on the volume of the microporous is raw < ACN13 < AC. This is also due to the same mass ratio between KOH and urea which inhibits pore formation, especially the micropore of carbon material produced from OPEFB. Pore size distribution shows that the porosity of activated carbon consists mainly of micropores and some mesopores. These micropores are formed by the release of non-carbon components such as N and O during carbonization, and also the use of KOH as an activating agent[44].

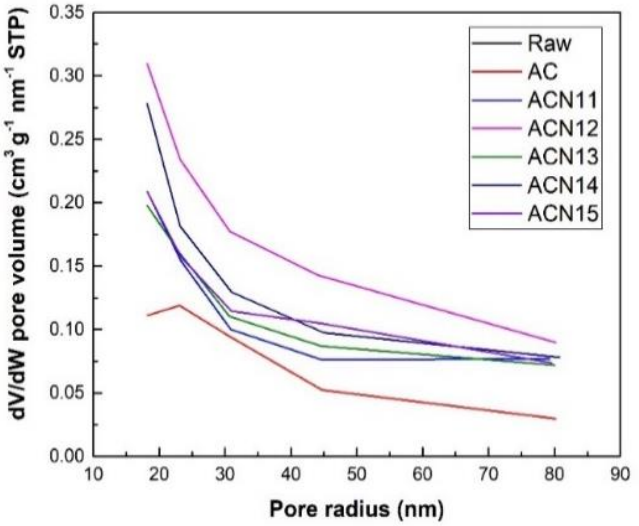

Figure 6. The pore size distribution (PSD) characteristics of carbon material from OPEFB using the BJH method

E. CO_2 adsorption

CO_2 adsorption capacity was tested using the gravimetric method for carbon, activated carbon, ACN11 and ACN14 samples at 30 °C. Before doing the adsorption, the carbon material sample is first degassed at 300 °C for 3 hours to remove pollutant gases in the pores of the carbon material [17], so that the adsorbed is pure CO_2 gas.

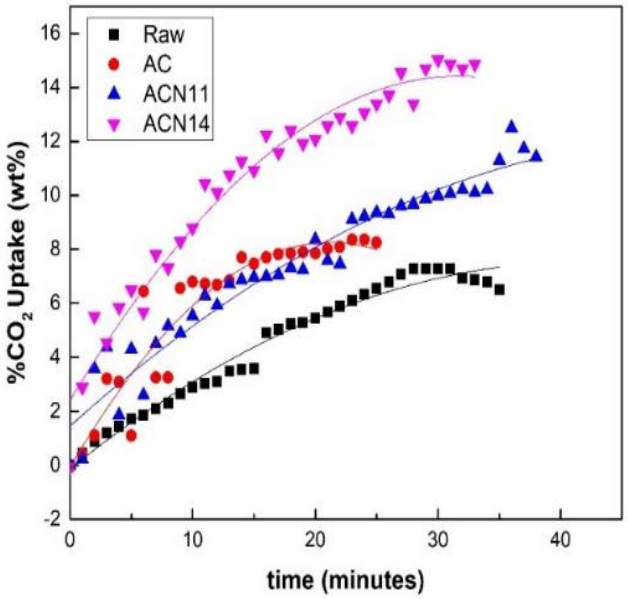

Figure 7. CO_2 adsorption capacity using carbon adsorbent (without activation and doping), activated carbon, ACN11, and ACN14

Figure 7 shows CO_2 adsorption capacity of carbon adsorbents, activated carbon, ACN11, and ACN14 at 7.29 wt%, 8.36 wt%, 12.67 wt% and 15.02 wt%, respectively. Based on the adsorption data of CO_2, carbon and activated carbon have differences because activated carbon is activated using KOH so that the pores in the activated carbon of OPEFB become open and micropores and some mesopores are formed[41]. This is also supported by the data presented in table 2. While the difference between activated carbon and ACN11 and ACN14 differed significantly because there was CO2-philic heteroatom nitrogen doping[43]. Although S_{BET} ACN11 > S_{BET} ACN14, the CO_2 adsorption capacity produced is greater than ACN11, because this amount of nitrogen inserted in the ACN14 sample is greater than ACN11. This proves that the more nitrogen mass added to the activated carbon, the greater the CO_2 adsorption capacity, but it should be noted that other factors such as the type of activating agent and the activating agent mass are added so that the addition of doping nitrogen heteroatoms is not inhibiting the CO_2 adsorptivity performance.

F. *Adsorption Kinetics Study*

In order to investigate the mechanism of adsorption rate for the adsorption of CO_2 by activated carbon derived from OPEFB, the rate constants were determined by applying eqn (2), (4), and (6).

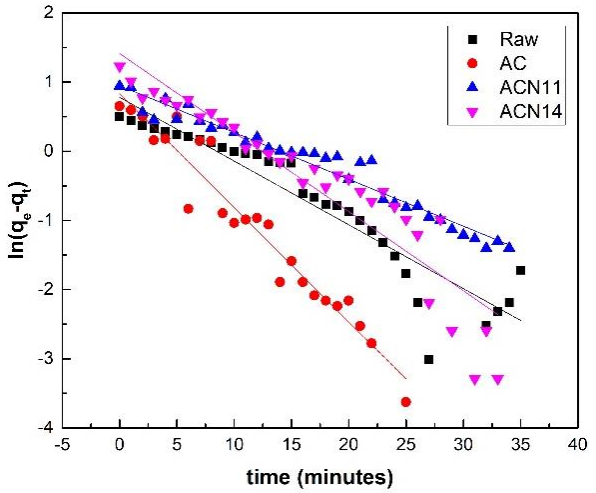

(a)

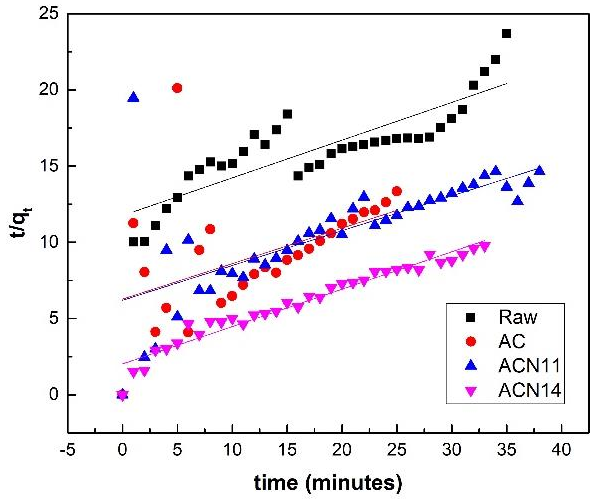

(b)

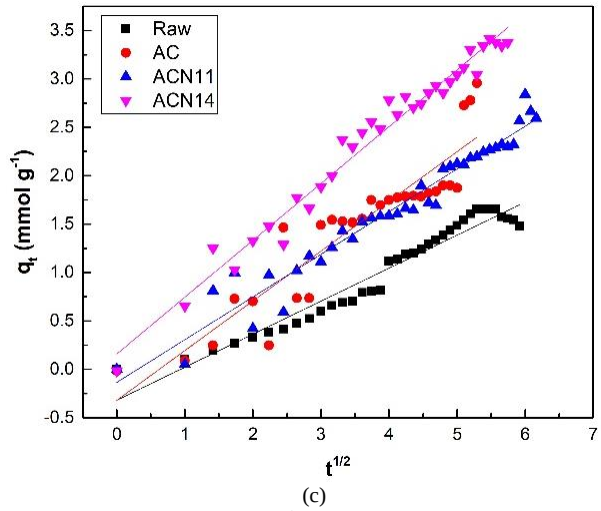

(c)

Figure 8. Kinetics model (a) pseudo-first order, (b) pseudo-second order, and (c) intraparticle diffusion for CO_2 adsorption in raw, AC, ACN11, and ACN14

The adsorption parameters for pseudo-first order, pseudo-second order, and intraparticle diffusion kinetics were determined from the plot ln (qe-qt) based on time t, plot t / qt with time t, and plot qt with $t^{1/2}$ is shown in Figure 8. Constant parameters and regression coefficients (R^2) are shown in Table 3. The results of straight-line analysis show the application of the pseudo-first order adsorption kinetics model, pseudo-second order, and change the intraparticle diffusion rate.

Table 3.
Comparison of the pseudo-first and pseudo-second order adsorption, and intraparticle diffusion rate constants of raw, AC, ACN11, and ACN14

Model	Parameter		
Pseudo-first order	k_f	q_e	R^2
Raw	-0.09	2.34	0.86
AC	-0.17	1.65	0.56
ACN11	-0.07	2.00	0.61
ACN14	-0.11	3.81	0.79

Model	Parameter		
Pseudo-second order	h	q_e	R^2
Raw	0.10	3.33	0.64
AC	0.13	9.80	0.09
ACN11	0.16	4.38	0.48
ACN14	0.50	4.08	0.95

Model	Parameter		
Intraparticle diffusion	k_{id}	C	R^2
Raw	0.34	-0.32	0.95
AC	0.63	-0.63	0.84
ACN11	0.44	-0.13	0.95
ACN14	0.59	0.16	0.97

The assumption used in the pseudo-first order model is the concentration of reactants in this case the adsorbate is much higher than the concentration of other reactants. The assumption used in the pseudo-second order model is the number of sites active on the surface of the adsorbent which is always the same as the adsorption capacity[45].

The difference can be seen in Figure 8c which shows two adsorption steps for ACN11 and ACN14, the first is external surface adsorption, or macropore diffusion and the last is internal surface adsorption or micropore diffusion. External diffusion occurs faster than internal diffusion[32]. The kinetic model suitable for raw materials, AC, ACN11 and ACN14 is the intraparticle diffusion. This can be seen from the R^2 values of raw, AC, ACN11, and ACN14, respectively 0.95, 0.84, 0.95, and 0.97. However, asking further, such as molecular modeling is needed for the phenomenon of the application.

IV. Conclusion

In this study the development of biomass-based adsorbent material has been successfully synthesized. OPEFB has the potential as a precursor for activated carbon because it produces a yield of 61.5 wt%. The activated carbon produced can be carried out using the single-step pyrolysis method at 800 °C using a KOH chemical activator because it produces S_{BET} of 699.14 m^2 g^{-1} with V_{micro} of 0.45 cm^3 g^{-1}. The development of activated carbon material by adding doping nitrogen heteroatoms can increase the surface area to reach 1309.47 m^2 g^{-1} and 1230.30 m^2 g^{-1} for ACN11 and ACN14, respectively. The increase in surface properties was followed by an increase in CO_2 adsorption capacity of 12.67 wt% and 15.02 wt% for ACN11 and ACN14, respectively. This is because the basic properties of nitrogen can attract CO_2 which is acidic by physisorption. The adsorption rate compares the raw and AC kinetics models, the results show that the same adsorption kinetics model for ACN11 and ACN14 follows

the adsorption model of intraparticle diffusion kinetics with R^2 values for ACN11 and ACN14 of 0.95 and 0.97, respectively.

REFERENCES

[1] T. R.Anderson, E. Hawkins, and P. D.Jones, "CO_2, the greenhouse effect and global warming: from the pioneering work of Arrhenius and Callendar to today's Earth System Models," *Endeavour*, vol. 40, no. 3, pp. 178–187, 2016.

[2] B. Ioan and L. Amelitta, "Carbon dioxide-significant emission sources and decreasing solutions," *Procedia - Soc. Behav. Sci.*, vol. 180, pp. 1122–1128, 2015.

[3] Q. Wang, J. Luo, Z. Zhong, and A. Borgna, "CO_2 capture by solid adsorbents and their applications: current status and new trends," *Energy Environ. Sci.*, vol. 4, no. 1, pp. 42–55, 2011.

[4] C. Stewart and M.-A. Hessami, "A study of methods of carbon dioxide capture and sequestration—the sustainability of a photosynthetic bioreactor approach," *Energy Convers. Manag. 2005, Pages*, vol. 46, no. 3, pp. 403–420, 2005.

[5] L. Li, N. Zhao, W. Wei, and Y. Sun, "A review of research progress on CO2 capture, storage, and utilization in Chinese Academy of Sciences," *Fuel*, vol. 108, pp. 112–130, 2013.

[6] P. N. Sutar, A. Jha, P. D.Vaidyaa, and E. Y. Kenig, "Secondary amines for CO_2 capture: A kinetic investigation using N-ethylmonoethanolamine," *Chem. Eng. J.*, no. 207–208, pp. 718–724, 2012.

[7] H. Liu *et al.*, "A hybrid absorption-adsorption method to efficiently capture carbon," *Nat. Commun.*, vol. 5, pp. 1–7, 2014.

[8] J. I. Eze and K. E. Agbo, "Maximizing the potentials of biogas through upgrading," *Am. J. Sci. Ind. Res.*, vol. 1, no. 3, pp. 604–609, 2010.

[9] A. Modak and S. Jana, "Advancement in porous adsorbents for post-combustion CO_2 capture," *Microporous and Mesoporous Materials*, vol. 276. Elsevier B.V., pp. 107–132, 01-Mar-2019.

[10] H. B. Nguyen *et al.*, "Graphene patterned polyaniline-based biosensor for glucose detection," *Adv. Nat. Sci. Nanosci. Nanotechnol.*, vol. 3, no. 2, Jun. 2012.

[11] R. S. Franchi, P. J. E. Harlick, and A. Sayari, "Applications of pore-expanded Mesoporous Silica. 2. Development of a high-capacity, water-tolerant adsorbent for CO_2," *Ind. Eng. Chem. Res.*, vol. 44, no. 21, pp. 8007–8013, Oct. 2005.

[12] L. Tan and B. Tan, "Hypercrosslinked porous polymer materials: Design, synthesis, and applications," *Chemical Society Reviews*, vol. 46, no. 11. Royal Society of Chemistry, pp. 3322–3356, 07-Jun-2017.

[13] M. R. Hudson, W. L. Queen, J. A. Mason, D. W. Fickel, R. F. Lobo, and C. M. Brown, "Unconventional, highly selective CO_2 adsorption in Zeolite SSZ-13," *J. Am. Chem. Soc.*, vol. 134, no. 4, pp. 1970–1973, Feb. 2012.

[14] A. Modak and A. Bhaumik, "Porous carbon derived via KOH activation of a hypercrosslinked porous organic polymer for efficient CO_2, CH_4, H_2 adsorptions and high CO_2/N_2 selectivity," *J. Solid State Chem.*, vol. 232, pp. 157–162, Dec. 2015.

[15] A. S. González, M. G. Plaza, F. Rubiera, and C. Pevida, "Sustainable biomass-based carbon adsorbents for post-combustion CO_2 capture," *Chem. Eng. J.*, vol. 230, pp. 456–465, Aug. 2013.

[16] D. Bonenfant, M. Kharoune, P. Niquette, M. Mimeault, and R. Hausler, "Advances in principal factors influencing carbon dioxide adsorption on zeolites," *Sci. Technol. Adv. Mater.*, vol. 9, no. 1, 2008.

[17] K. Kim, M. Choi, and R. Ryoo, "Ethanol-based synthesis of hierarchically porous carbon using nanocrystalline beta zeolite template for high-rate electrical double layer capacitor," *Carbon N. Y.*, vol. 60, pp. 175–185, Aug. 2013.

[18] S. J. Yang, H. Jung, T. Kim, and C. R. Park, "Recent advances in hydrogen storage technologies based on nanoporous carbon materials," *Prog. Nat. Sci. Mater. Int.*, vol. 22, no. 6, pp. 631–638, 2012.

[19] B. O. Evbuomwan, A. M. Agbede, and M. M. Atuka, "A comparative study of the physico-chemical properties of activated carbon from oil palm paste (kernel shell and fibre)," *Int. J. Sci. Eng. Investig.*, vol. 2, no. 19, pp. 75–79, 2013.

[20] K. Hussaro, "Preparation of activated carbon from palm oil shell by chemical activation with Na_2CO_3 and $ZnCl_2$ as impregnated agents for H2S adsorption," *Am. J. Environ. Sci.*, vol. 10, no. 4, pp. 336–346, 2014.

[21] A. S. Ello, L. K. C. De Souza, A. Trokourey, and M. Jaroniec, "Development of microporous carbons for CO_2 capture by KOH activation of African palm shells," *J. CO2 Util.*, vol. 2, pp. 35–38, 2013.

[22] J. Guo and A. C. Lua, "Textural and chemical properties of adsorbent prepared from palm shell by phosphoric acid activation," *Mater. Chem. Phys.*, vol. 80, no. 1, pp. 114–119, Apr. 2003.

[23] K. Y. Foo and B. H. Hameed, "Adsorption characteristics of industrial solid waste derived activated carbon prepared by microwave heating for methylene blue," *Fuel Process. Technol.*, vol. 99, pp. 103–109, Jul. 2012.

[24] R. Farma *et al.*, "Preparation of highly porous binderless activated carbon electrodes from fibres of oil palm empty fruit bunches for application in supercapacitors," *Bioresour. Technol.*, vol. 132, pp. 254–261, 2013.

[25] Z. Rouzitalab, D. Mohammady Maklavany, A. Rashidi, and S. Jafarinejad, "Synthesis of N-doped nanoporous carbon from walnut shell for enhancing CO_2 adsorption capacity and separation," *J. Environ. Chem. Eng.*, vol. 6, no. 5, pp. 6653–6663, Oct. 2018.

[26] Z. Liu, Y. Zhu, Z. Du, W. Xing, S. Komarneni, and Z. Yan, "Detailed investigation of N-doped microporous carbons derived from urea furfural resin for CO_2 capture," *J. Porous Mater.*, vol. 22, no. 6, pp. 1663–1672, Dec. 2015.

[27] Isroi *et al.*, "Structural Changes of Oil Palm Empty Fruit Bunch (OPEFB) after Fungal and Phosphoric Acid Pretreatment," *Molecules*, vol. 17, no. 12, pp. 14995–15012, Dec. 2012.

[28] C.-H. Ooi, T. Lee, S.-Y. Pung, and F.-Y. Yeoh, "Activated carbon fiber derivied from single step carbonization-activation process," 2013.

[29] E. Redondo *et al.*, "Outstanding room-temperature capacitance of biomass-derived microporous carbons in ionic liquid electrolyte," *Electrochem. commun.*, vol. 79, pp. 5–8, Jun. 2017.

[30] M. Delavar, A. A. Ghoreyshi, M. Jahanshahi, S. Khalili, and N. Nabian, "The effect of chemical treatment on adsorption of natural gas by multi-walled carbon nanotubes: Sorption equilibriaand thermodynamic studies," *Chem. Ind. Chem. Eng. Q.*, vol. 18, no. 2, pp. 193–207, 2012.

[31] T. Gunawan, R. Wijiyanti, and N. Widiastuti, "Adsorption-desorption of CO_2 on zeolite-Y-templated carbon at various temperatures," *RSC Adv.*, vol. 8, no. 72, pp. 41594–41602, 2018.

[32] N. Widiastuti, H. Wu, H. M. Ang, and D. Zhang, "Removal of ammonium from greywater using natural zeolite," *Desalination*, vol. 277, no. 1–3, pp. 15–23, Aug. 2011.

[33] A. Shiue, S.-C. Hu, S.-M. Chang, T.-Y. Ko, A. Hsieh, and A. Chan, "Adsorption kinetics and breakthrough of carbon dioxide for the chemical modified activated carbon filter used in the building," *Sustainability*, vol. 9, no. 9, pp. 1–13, 2017.

[34] S. Sutikno, M. Marniza, N. Nawansih, and F. Feriandi, "Teknik perlakuan awal dan sakarifikasi tandan kosong kelapa sawit menjadi gula reduksi sebagai bahan baku produksi bioetanol," 2017, pp. 1339–1346.

[35] C. Rodriguez Correa, T. Otto, and A. Kruse, "Influence of the biomass components on the pore formation of activated carbon," *Biomass and Bioenergy*, vol. 97, pp. 53–64, 2017.

[36] J. Guo, B. Gui, S. X. Xiang, X. T. Bao, H. J. Zhang, and A. C. Lua, "Preparation of activated carbons by utilizing solid wastes from palm oil processing mills," *J. Porous Mater.*, vol. 15, no. 5, pp. 535–540, Oct. 2008.

[37] N. S. Nasri, U. D. Hamza, S. N. Ismail, M. M. Ahmed, and R. Mohsin, "Assessment of porous carbons derived from sustainable palm solid waste for carbon dioxide capture," in *Journal of Cleaner Production*, 2014, vol. 71, pp. 148–157.

[38] A. R. Hidayu, N. F. Mohamad, S. Matali, and A. S. A. K. Sharifah, "Characterization of activated carbon prepared from oil palm empty fruit bunch using BET and FT-IR techniques," in *Procedia Engineering*, 2013, vol. 68, pp. 379–384.

[39] Y. Xia, Z. Yang, X. Gou, and Y. Zhu, "A simple method for the production of highly ordered porous carbon materials with increased hydrogen uptake capacities," *Int. J. Hydrogen Energy*, vol. 38, no. 12, pp. 5039–5052, Apr. 2013.

[40] M. Zhang *et al.*, "Improving biomass-derived carbon by activation with nitrogen and cobalt for supercapacitors and oxygen reduction reaction," *Appl. Surf. Sci.*, vol. 411, pp. 251–260, Jul. 2017.

[41] K. Li *et al.*, "Mechanism of biomass activation and ammonia modification for nitrogen-doped porous carbon materials," *Bioresour. Technol.*, vol. 280, pp. 260–268, May 2019.

[42] S. D. Yim *et al.*, "Decomposition of Urea into NH_3 for the SCR Process," *Ind. Eng. Chem. Res.*, vol. 43, no. 16, pp. 4856–4863, Aug. 2004.

[43] H. B. H. Cooper and H. W. Spencer III, "US6730280B2 - Methods for the production of ammonia from urea and/or biuret, and uses for NOx and/or particulate matter removal - Google Patents," 2004.

[44] A. Alabadi, S. Razzaque, Y. Yang, S. Chen, and B. Tan, "Highly porous activated carbon materials from carbonized biomass with high CO_2 capturing capacity," *Chem. Eng. J.*, vol. 281, pp. 606–612, Dec. 2015.

[45] B. S. Çağlayan and A. E. Aksoylu, "CO_2 adsorption behavior and kinetics on chemically modified activated carbons," *Turkish J. Chem.*, vol. 40, no. 4, pp. 576 – 587, 2016.